Circulation

ORIGINAL RESEARCH ARTICLE

P16+ Cells Drive Adverse Postischemic Cardiac Remodeling Through CCL8-Mediated Recruitment of Cytotoxic Lymphocytes

Lei Yan, PhD*; Jialei Zheng, BS*; Zhengkai Lu, PhD*; Anqi Zhu, BS; Min Ye, BS; Jufeng Meng, MS; Juan Tang, PhD†; Hui Zhang, PhD†

BACKGROUND: Ischemic heart disease remains a leading cause of mortality worldwide, with adverse remodeling after myocardial infarction driven by inflammation and cardiomyocyte loss. Although cytotoxic lymphocytes exacerbate myocardial injury and P16 marks cellular senescence in diseased hearts, the cell type–specific functions of P16+ populations remain unclear.

METHODS: Using *p16-CreER;R26-tdT* reporter mice, we mapped P16+ cell heterogeneity after myocardial infarction. Senolytic effects were assessed with combined dasatinib and quercetin treatment. Transcriptomic profiling (bulk and single-cell RNA sequencing) of sorted P16+ cells identified secreted factors, validated through in silico predictions and quantitative polymerase chain reaction. Intercellular communication was analyzed using CellChat. Functional relevance was tested through CCL8 (cytokine [C-C motif] ligand 8) neutralization, *Ccl8* deletion in P16+ cells, lymphocyte depletion, and intersectional genetic ablation of P16+ fibroblasts or macrophages using dual-recombinase systems (*p16-DreER;Pdgfra-CreER;R26-lr-tdT-DTR* and *p16-DreER;Cx3cr1-CreER;R26-lr-tdT-DTR*).

RESULTS: P16 was induced in fibroblasts, macrophages, coronary endothelial cells, and cardiomyocytes after myocardial infarction. Dasatinib and quercetin treatment selectively eliminated P16+ macrophages and fibroblasts, improving cardiac function. Transcriptomic analysis identified P16+ fibroblasts and macrophages as the main sources of CCL8. CCL8 blockade reduced infiltration of cytotoxic lymphocytes (CD8+ T cells and natural killer cells), decreased cardiomyocyte apoptosis, and enhanced repair. Genetic deletion of *Ccl8* in P16+ cells reproduced these benefits. It is important to note that ablation of P16+ fibroblasts, but not macrophages, diminished fibrosis and improved function, and depletion of CD8+ T cell attenuated adverse remodeling.

CONCLUSIONS: P16+ cells orchestrate maladaptive remodeling after myocardial infarction through CCL8-dependent recruitment of cytotoxic lymphocytes, particularly CD8+ T cells, which drive cardiomyocyte apoptosis. Targeting P16+ fibroblasts or blocking CCL8 offers a promising therapeutic approach for ischemic heart disease.

Key Words: CCL8 ■ cytotoxic lymphocytes ■ myocardial infarction ■ P16

Ischemic heart disease is a leading global cause of morbidity and mortality.[1] Acute interruption of myocardial perfusion initiates pathological cascades—including inflammation, fibrosis, and cardiomyocyte death—that collectively drive adverse cardiac remodeling and, if unresolved, progress to heart failure.[2,3] Elucidating the mechanisms underlying postischemic cardiac remodeling is therefore crucial for both mechanistic insight and therapeutic innovation.

After ischemic injury, diverse innate and adaptive immune cell subsets infiltrate the myocardium, exerting either protective or deleterious effects depending on

Correspondence to: Hui Zhang, PhD, School of Life Science and Technology & State Key Laboratory of Advanced Medical Materials and Devices, ShanghaiTech University, 393 Middle Huaxia Road, Pudong, Shanghai 201210, China, Email zhanghui1@shanghaitech.edu.cn; or Juan Tang, PhD, State Key Laboratory of Cardiovascular Diseases and Medical Innovation Center, Shanghai East Hospital, Frontier Science Center for Stem Cell Research, School of Life Science and Technology, Tongji University, Shanghai 200092, China, Email tangjuan@tongji.edu.cn
*L. Yan, J. Zheng, and Z. Lu contributed equally.
†J. Tang and H. Zhang contributed equally.
Supplemental Material is available at https://www.ahajournals.org/doi/suppl/10.1161/CIRCULATIONAHA.125.077172.

Circulation is available at www.ahajournals.org/journal/circ

ORIGINAL RESEARCH ARTICLE

Clinical Perspective

What Is New?

- This study provides a systematic characterization of P16+ cellular heterogeneity in the heart after myocardial infarction.
- CCL8 (cytokine [C-C motif] ligand 8) is identified as a critical secreted factor from P16+ macrophages and fibroblasts that drives adverse remodeling by recruiting cytotoxic lymphocytes.
- Using intersectional genetics, selective ablation of P16+ fibroblasts, but not macrophages, improves cardiac repair after myocardial infarction.

What Are the Clinical Implications?

- CCL8 blockage emerges as a novel immunomodulatory strategy to mitigate cytotoxic lymphocyte–mediated injury and adverse remodeling after myocardial infarction.
- These findings advocate moving beyond broad senolysis toward precision targeting of pathogenic subsets, specifically P16+ cardiac fibroblasts, to disrupt a key node in the maladaptive repair network.

Nonstandard Abbreviations and Acronyms

CAR	chimeric antigen receptor
c-CASP3	cleaved caspase 3
CCL8	cytokine (C-C motif) ligand 8
cVEC	coronary vascular endothelial cell
DQ	dasatinib and quercetin
DTR	diphtheria toxin receptor
GZMB	granzyme B
IL	interleukin
MI	myocardial infarction
NK	natural killer
SASP	senescence-associated secretory phenotype
scRNA-seq	single-cell RNA sequencing
TGF-β	transforming growth factor β
TNFα	tumor necrosis factor α

their phenotype and temporal activation.[4] Among them, T lymphocytes (T cells) play essential roles in postischemic cardiac remodeling.[5–7] T cells are broadly divided into CD4+ and CD8+ subsets, with distinct effects on myocardial injury and repair. In permanent left anterior descending coronary artery ligation models, both conventional and regulatory CD4+ T cells are activated after myocardial infarction (MI).[8] In this context, CD4+ T cell activation promotes wound healing and survival through self-antigen recognition, whereas CD4+ T cell–deficient mice exhibit worsened left ventricular dilation, impaired collagen deposition, and higher mortality.[8] Furthermore, regulatory CD4+ T cells further facilitate healing by modulating monocyte/macrophage differentiation.[9]

CD8+ T cells also infiltrate the heart after coronary artery occlusion in rodents and are equally as abundant as CD4+ T cells in ischemic failing human hearts.[10–12] Post-MI CD8+ T cells display cytotoxic activity against normal cardiomyocytes in vitro[10] and produce high levels of cytotoxic mediators, such as perforin and GZMB (granzyme B).[12] The perforin–granzyme pathway, a key mechanism by which cytotoxic lymphocytes induce apoptosis, plays a critical role in immune defense, tumor surveillance, and tissue homeostasis.[13] Recent evidence indicates that CD8+ T cells recruited to the ischemic myocardium promote cardiomyocyte death through GZMB release, exacerbating inflammation, tissue injury, and cardiac functional deterioration.[14]

Natural killer (NK) cells, another cytotoxic lymphocyte subset that employs the perforin–granzyme pathway,[13] have also been implicated in cardiac pathology, although their role in MI remains incompletely defined.[15–17] NK cell cytotoxicity is reduced in the peripheral blood of patients with MI and murine models, yet these cells may still contribute to myocardial remodeling by lysing damaged cells or modulating inflammation through cytokine release.[18,19]

P16, a cyclin-dependent kinase inhibitor protein encoded by *Cdkn2a* (also known as $p16^{INK4a}$), is widely used as a senescence marker. P16 expression is rarely detected in young, healthy tissues, but accumulates in aged and diseased organs.[20–26] Reporter models driven by the *p16* promoter have been instrumental in tracking senescent cells.[20–26] Removal of P16+ cells through genetic ablation or senolytics such as ABT263 (also known as navitoclax) or dasatinib and quercetin (DQ) has demonstrated diverse physiological and pathological effects across tissues.[27–29] The impact of P16+ cells is context- and cell type–dependent, varying between aging, disease, and regeneration.

Senolytic studies suggest a role for P16+ cells in post-MI cardiac remodeling.[30,31] For instance, ABT263 eliminated P16+ cells after ischemia–reperfusion MI, reducing scar size, enhancing angiogenesis, and improving cardiac function.[32] Yet systematic characterization of P16+ cardiac populations after MI remains incomplete, and the cell type–specific mechanisms through which P16+ cells influence remodeling are poorly understood.

Here we show that P16 is induced in multiple cardiac cell populations—including fibroblasts, macrophages, coronary vascular endothelial cells (cVECs), and cardiomyocytes—after MI. Senolytic DQ selectively removed P16+ macrophages and fibroblasts, improving cardiac repair. Bulk and single-cell transcriptomics combined with intercellular communication analyses identified P16+ macrophages and fibroblasts as major producers of CCL8 (cytokine [C-C motif] ligand 8), which recruits

cytotoxic CD8+ T cells and NK cells to promote adverse cardiac remodeling. It is important to note that genetic ablation of P16+ fibroblasts, but not P16+ macrophages, reduced scar area and improved cardiac function. These findings highlight CCL8 blockade and fibroblast-specific elimination of P16+ cells as promising strategies for treating ischemic heart disease.

METHODS

The data supporting this study are available from the corresponding author upon reasonable request. The primers and antibodies used in this study are listed in Tables S1 and S2, respectively. Detailed methods are provided in the Supplemental Material.

Animal Experiments

All procedures were approved by the Institutional Animal Care and Use Committee at ShanghaiTech University (Shanghai, China). Mice were maintained under controlled temperature and humidity with a 12-hour light/12-hour dark cycle and ad libitum access to water and standard chow. Investigators performing surgeries and subsequent echocardiography were blinded to group allocation throughout data collection and analysis.

Statistical Analysis

Quantitative data represent at least 3 independent biological replicates and are presented as mean ± SEM. The Shapiro-Wilk test was used to ensure that the data were distributed normally, and $P \geq 0.05$ was interpreted as consistent with a normal distribution. Comparisons between 2 groups were performed with a 2-tailed Student *t* test. For comparisons among 3 or more groups with a single independent variable, 1-way ANOVA followed by the Tukey multiple comparisons test was used. A 2-sided $P<0.05$ was considered statistically significant. Analyses were performed using GraphPad Prism (version 10.3.1; GraphPad Inc), with blinding maintained throughout data processing.

Data and Code Availability

Raw single-cell RNA sequencing (scRNA-seq) and bulk RNA sequencing datasets have been deposited in the Gene Expression Omnibus and are publicly available at publication. The scRNA-seq data were deposited at GSE303571. The bulk RNA sequencing data were deposited at GSE305646. Additional information required for reanalysis is available from the corresponding author upon request. No unique code was generated.

RESULTS

P16+ Cellular Heterogeneity in the Myocardium After MI

To define the identify of P16+ cells after MI, we generated a *p16-CreER* knock-in mouse by inserting a 2A-CreER cassette into the terminal exon upstream of the stop codon in the endogenous *Cdkn2a* locus (Figure 1A). The self-cleaving 2A peptide enables concurrent expression of P16 and CreER. *p16-CreER* mice were crossed with *Rosa26-loxP-Stop-loxP-tdTomato* reporter mice (hereafter *R26-tdT*) to obtain *p16-CreER;R26-tdT* animals.[33]

Because P16+ cells accumulate with age, *p16-CreER;R26-tdT* mice aged 2, 6, and 12 months were treated with tamoxifen and harvested 48 hours later. Immunofluorescence showed age-progressive accumulation of tdTomato+ cells in multiple organs, including heart, lung, spleen, liver, intestine, and kidney (Figure S1A and S1B). Coimmunostaining of lung and spleen with anti-tdTomato and anti-P16 confirmed concordant expression (Figure S1C through S1F), validating tdTomato as a faithful surrogate for endogenous P16.

We next characterized P16+ cellular heterogeneity in the post-MI heart. Adult *p16-CreER;R26-tdT* mice (2 months old) underwent permanent left anterior descending coronary artery ligation. A single dose of tamoxifen was given at 5 days after MI, and hearts were analyzed at 7 days after MI. Sparse tdTomato+ cells were present in remote myocardium, whereas dense labeling appeared within infarct zones (Figure 1B). tdTomato+ cells colocalized with P16 in injured myocardium (Figure 1B). Cell type analysis within injured regions identified tdTomato+ PDGFRa+ fibroblasts (Figure 1C), CDH5+ cVECs (Figure 1D), F4/80+ macrophages (Figure 1E), and TNNI3+ cardiomyocytes (Figure 1F), indicating endogenous *p16* activation in these populations. Flow cytometry of infarct tissues at 7 days after MI showed tdTomato labeling in both Ly6C^{high} (inflammatory) and Ly6C^{low} (reparative) macrophage subsets (Figure S2A). Immunostaining further identified tdTomato+ARG1+ M2-like macrophages in injured areas (Figure S2B). Validation in wild-type mice by costaining confirmed P16 expression in fibroblasts, cVECs, macrophages, and cardiomyocytes within infarct regions at 7 days after MI (Figure 1G through 1J).

To assess persistence of P16 expression at later stages, *p16-CreER;R26-tdT* mice received tamoxifen at 26 days after MI and were analyzed 48 hours later. Costaining demonstrated ongoing P16 activation in fibroblasts, cardiomyocytes, macrophages, and cVECs in chronic infarcts (Figure S3), underscoring sustained P16+ cellular heterogeneity during long-term cardiac remodeling.

DQ Treatment Selectively Eliminates P16+ Macrophages and Fibroblasts After MI

Senolytics remove P16+ cells across tissues, but their cell type specificity and impact on post-MI repair are incompletely defined. To address this, we administered DQ or vehicle to wild-type mice every 4 days after MI and analyzed outcomes at 28 days. Compared with controls, DQ-treated mice exhibited improved cardiac function (Figure 2A; Figure S4A) and a reduced fibrotic scar area (Figure 2B and 2C). The decrease in overall heart

ORIGINAL RESEARCH ARTICLE

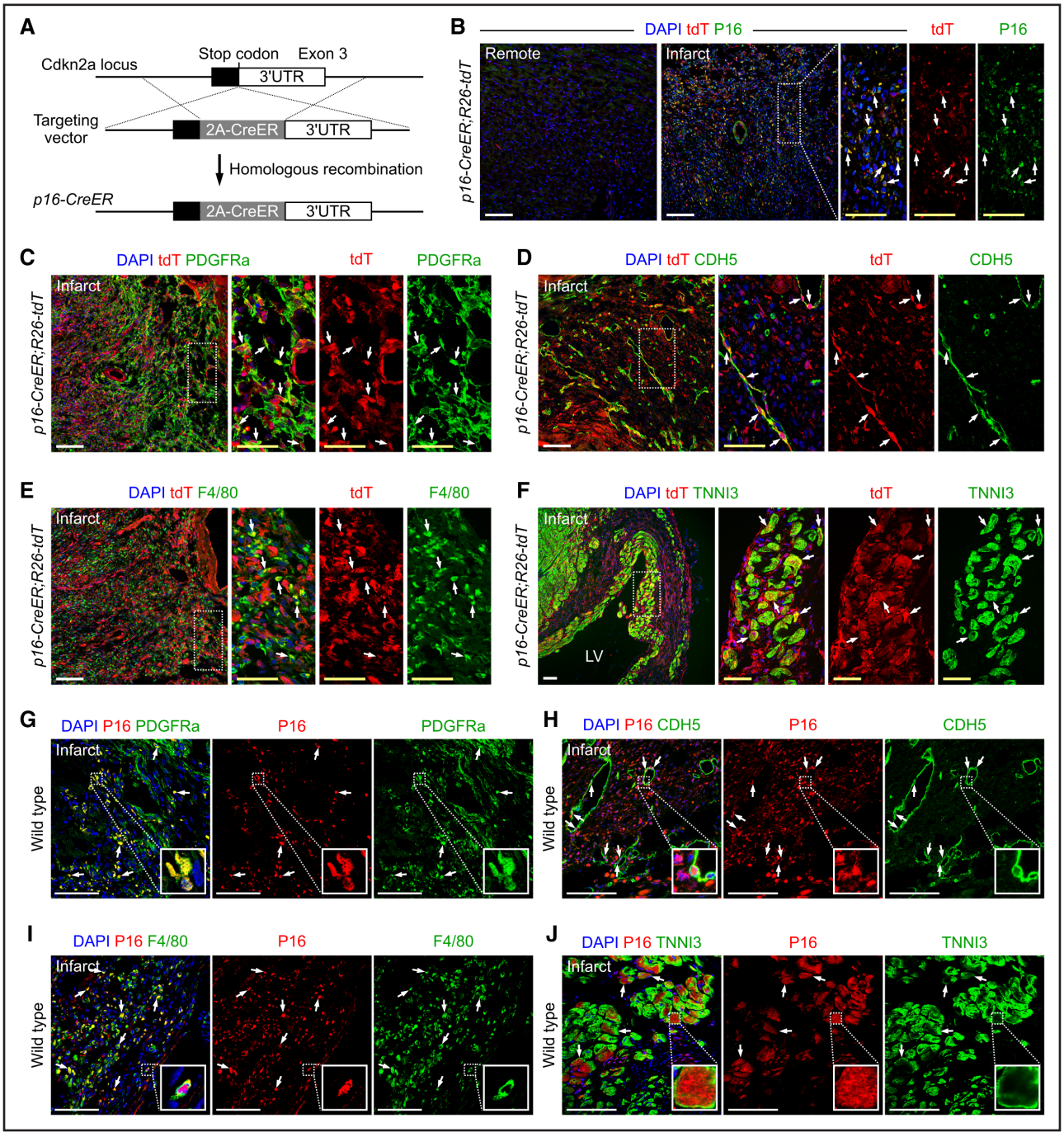

Figure 1. P16⁺ cellular heterogeneity in post-MI myocardium.
A, Strategy for generating the *p16-CreER* knock-in allele. **B**, *p16-CreER;R26-tdT* labels P16⁺ cells in infarct zones at 7 days after MI. **C** through **F**, *p16-CreER;R26-tdT* labels PDGFRa⁺ fibroblasts (**C**), CDH5⁺ endothelial cells (**D**), F4/80⁺ macrophages (**E**), and TNNI3⁺ cardiomyocytes (**F**) in injured regions at 7 days after MI. Arrows in **C** through **F** indicate tdTomato⁺ cells of respective lineage. **G** through **J**, P16 is detected in fibroblasts (**G**), endothelial cells (**H**), macrophages (**I**), and cardiomyocytes (**J**) in injured regions at 7 days after MI. Arrows in **G** through **J** indicate P16⁺ cells of respective lineage. White scale bars, 100 μm; yellow scale bars, 50 μm. MI indicates myocardial infarction.

size indicated an attenuation of post-MI hypertrophy (Figure 2B). Immunostaining revealed fewer P16⁺ cells within infarcts after DQ treatment (Figure 2D), corroborated by significantly reduced *p16* expression in infarct tissue (Figure 2E). Collectively, DQ treatment promotes cardiac repair after MI.

We then identified which P16⁺ subsets were ablated by DQ. *p16-CreER;R26-tdT* mice received DQ or vehicle every 4 days after MI, followed by tamoxifen at 26 days after MI; hearts were harvested 48 hours later (Figure 2F). Analysis of tdTomato-labeled cells revealed comparable densities of tdTomato⁺ cVECs and

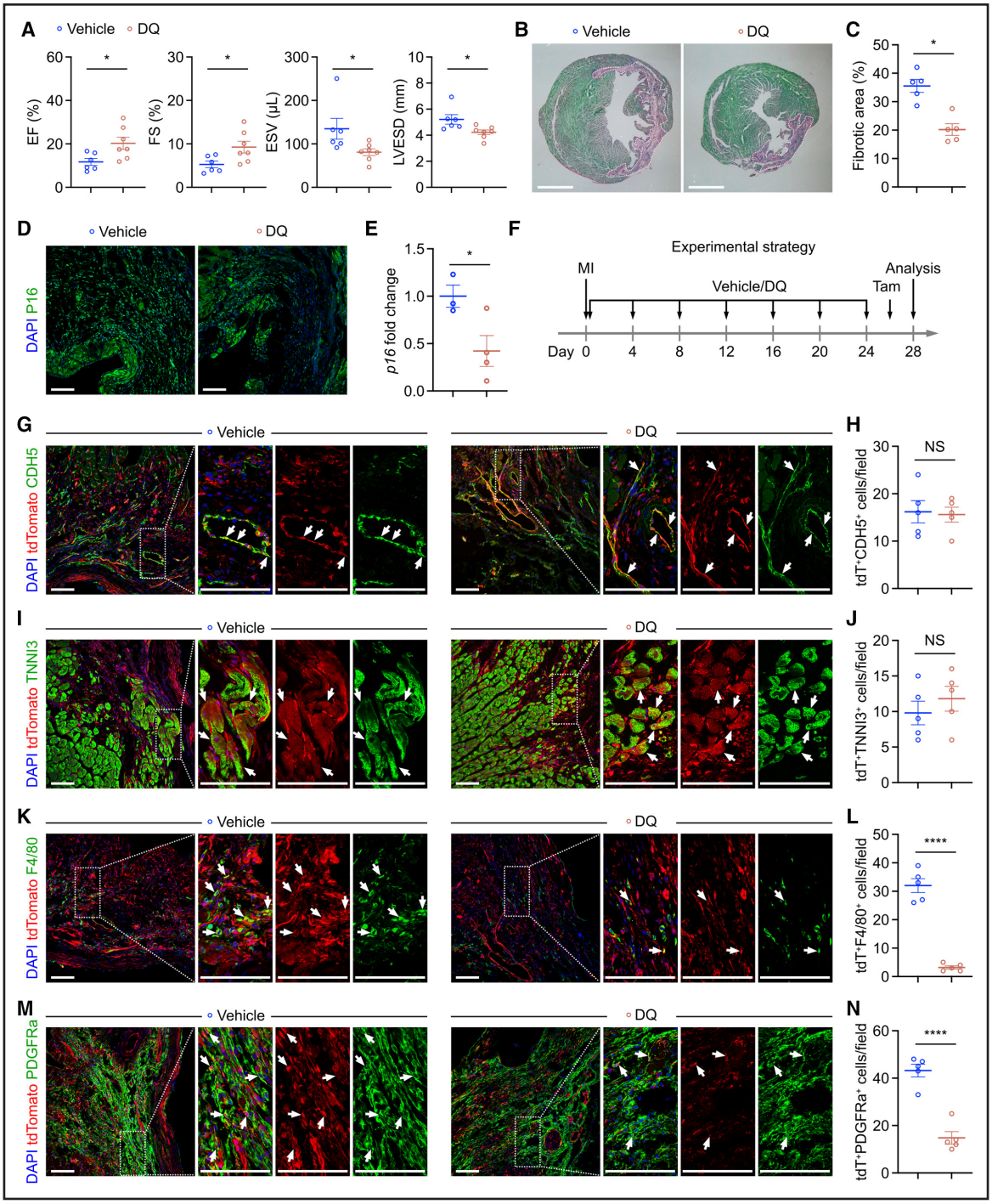

Figure 2. Senolytic treatment improves cardiac repair and eliminates P16⁺ macrophages and fibroblasts after MI.
A, DQ treatment (dasatinib, 5 mg/kg; quercetin, 50 mg/kg, every 4 days) improves cardiac function after MI. n=6 (vehicle), 7 (DQ); *$P<0.05$ (2-tailed Student *t* test). Both sexes were included. **B**, DQ treatment reduces fibrotic scar area (delineated by dashed line) after MI. Scale bars, 2 mm. **C**, Percentage of fibrotic area in injured hearts with vehicle or DQ treatment. n=5 per group; *$P<0.05$ (2-tailed Student *t* test). Both sexes were included. **D**, Immunostaining for P16 in injured sites. Scale bars, 100 μm. **E**, Fold change of *p16* expression in infarct tissues. n=3 or 4 per group; *$P<0.05$ (2-tailed Student *t* test). Both sexes were included. **F**, Schematic of the experimental strategy for detecting *p16-CreER;R26-tdT* targeted cells in injured sites with vehicle or DQ treatment. **G**, **I**, **K**, and **M**, tdTomato-labeled endothelial cells (**G**), cardiomyocytes (**I**), macrophages (**K**), and fibroblasts (**M**) in injured regions. Arrows indicate tdTomato⁺ cells of respective lineage. Scale bars, 100 μm. **H**, **J**, **L**, and **N**, Quantification of tdTomato⁺ endothelial cells (**H**), cardiomyocytes (**J**), macrophages (**L**), and fibroblasts (**N**) in injured regions. n = 5 per group; NS, nonsignificant; ****$P<0.0001$ (2-tailed Student *t* test). Both sexes were included. DQ indicates dasatinib and quercetin; EF, ejection fraction; ESV, end-systolic volume; FS, fractional shortening; LVESD, left ventricular end-systolic dimension; and MI, myocardial infarction.

cardiomyocytes between groups in injured regions (Figure 2G through 2J). In contrast, DQ significantly reduced tdTomato+ macrophage and fibroblast densities within infarcts (Figure 2K through 2N). Consistently, immunostaining revealed increased apoptosis of macrophages and fibroblasts in DQ-treated infarct areas (Figure S4B through S4E). Collectively, these data demonstrate that DQ selectively eliminates P16+ macrophages and fibroblasts after MI.

To further validate this finding by flow cytometry, we crossed *p16-CreER* mice with *Rosa26-loxP-mTomato-loxP-mGFP* (*R26-mTmG*) reporter mice to generate *p16-CreER;R26-mTmG* animals.[34] After MI, these mice received DQ or vehicle every 4 days and were given tamoxifen at 26 days after MI to label P16+ cells, and hearts were harvested 48 hours later. Flow-cytometric analysis confirmed that DQ treatment eliminated P16+ macrophages and fibroblasts in the post-MI hearts (Figure S4F through S4I).

To exclude the possibility that insufficient dosing accounted for the lack of clearance of P16+ cVECs and cardiomyocytes after MI, we tested intensified DQ dosing regimens (shortened intervals or increased doses) in *p16-CreER;R26-tdT* mice after infarction (Figure S5A through S5C). Immunofluorescence analysis demonstrated that even with these modified regimens, the densities of tdTomato+ cVECs and cardiomyocytes in infarct regions were not significantly reduced (Figure S5D through S5O).

CCL8 Upregulation in P16+ Macrophages and Fibroblasts After MI

Because DQ selectively eliminates P16+ macrophages and fibroblasts while improving repair after MI, we hypothesized that these populations drive maladaptive remodeling and represent therapeutic targets. To identify shared mechanisms by which P16+ macrophages and fibroblasts promote pathology, we interrogated their common secretory programs after MI.

To isolate P16+ macrophages and fibroblasts, *p16-CreER;R26-mTmG* mice were administered tamoxifen at 5 days after MI, and hearts were harvested at 7 days for flow cytometry sorting. GFP^{high} and GFP^{low} macrophages were sorted for bulk RNA sequencing (Figure 3A and 3B), identifying 981 differentially expressed genes between subsets: 106 downregulated and 875 upregulated in GFP^{high} macrophages (Figure 3C). Expression of key pro- and anti-inflammatory factors did not differ significantly between GFP^{high} and GFP^{low} macrophages (Figure S6A). Similarly, GFP^{high} and GFP^{low} fibroblasts were isolated from injured tissue (Figure 3D and 3E), yielding 1239 differentially expressed genes by RNA sequencing (432 downregulated; 807 upregulated) in GFP^{high} fibroblasts (Figure 3F). Compared with GFP^{low} fibroblasts, GFP^{high} fibroblasts did not show significant differences in the expression of cytoskeletal genes that serve as myofibroblast markers (Figure S6B), key profibrotic factors (Figure S6C), or major extracellular matrix genes (Figure S6D), indicating that GFP^{high} fibroblasts do not exhibit a more activated or profibrotic state.

Cross-comparison revealed 332 genes coordinately upregulated in both GFP^{high} macrophages and fibroblasts (Figure 3G). We then predicted shared secreted factors among these 332 coupregulated genes. Sequential bioinformatic filtering nominated candidate secreted proteins if they possessed a predicted N-terminal endoplasmic reticulum–targeting signal peptide, lacked predictable transmembrane domains, and were devoid of intracellular localization motifs (eg, endoplasmic reticulum retention signals, mitochondrial targeting peptides, nuclear export signals) (Figure 3H). This pipeline identified 12 candidate secreted proteins upregulated in both GFP^{high} macrophages and fibroblasts after MI (Figure 3H).

Quantitative polymerase chain reaction of infarcted versus remote myocardium at 7 days after MI revealed significant upregulation of only 2 candidates: *Ccl8* and epidermal growth factor–like domain 7 (*Egfl7*) (Figure 3I). Immunostaining confirmed markedly higher CCL8 protein levels in infarct zones compared with sham hearts or remote myocardial regions (Figure S7A and S7B). In *p16-CreER;R26-tdT* hearts harvested 7 days after MI, CCL8 protein was clearly detected in tdTomato+ macrophages and fibroblasts within injured areas, whereas expression in tdTomato+ cVECs and cardiomyocytes was negligible (Figure S7C through S7G). Although dysregulated CCL8 has been implicated in infectious, inflammatory, and neoplastic diseases, its role in post-MI cardiac remodeling remains undefined. We therefore focused subsequent investigation on CCL8 in the infarcted heart.

CCL8-Mediated Intercellular Communication Pathways in Hearts After MI

To delineate CCL8-centered signaling, we performed scRNA-seq on GFP^{high} and GFP^{low} noncardiomyocytes isolated from 3 *p16-CreER;R26-mTmG* mouse hearts at 7 days after MI. After quality control, 11 027 GFP^{low} and 9013 GFP^{high} cells remained. Uniform manifold approximation and projection identified 7 clusters—macrophages, fibroblasts, endothelial cells, T cells, vascular mural cells, B cells, and NK cells—each expressing established lineage markers (Figure 4A through 4C). Relative to GFP^{low} clusters, GFP^{high} populations contained a higher fraction of *Ccl8*-expressing cells, predominantly macrophages and fibroblasts, corroborating that CCL8 is selectively upregulated in P16+ macrophages and fibroblasts after MI (Figure 4D and 4E).

We next inferred intercellular communication using CellChat.[35] Integrated analyses revealed extensive signaling networks for both GFP^{high} and GFP^{low} macrophages in post-MI hearts (Figure S8A), including robust

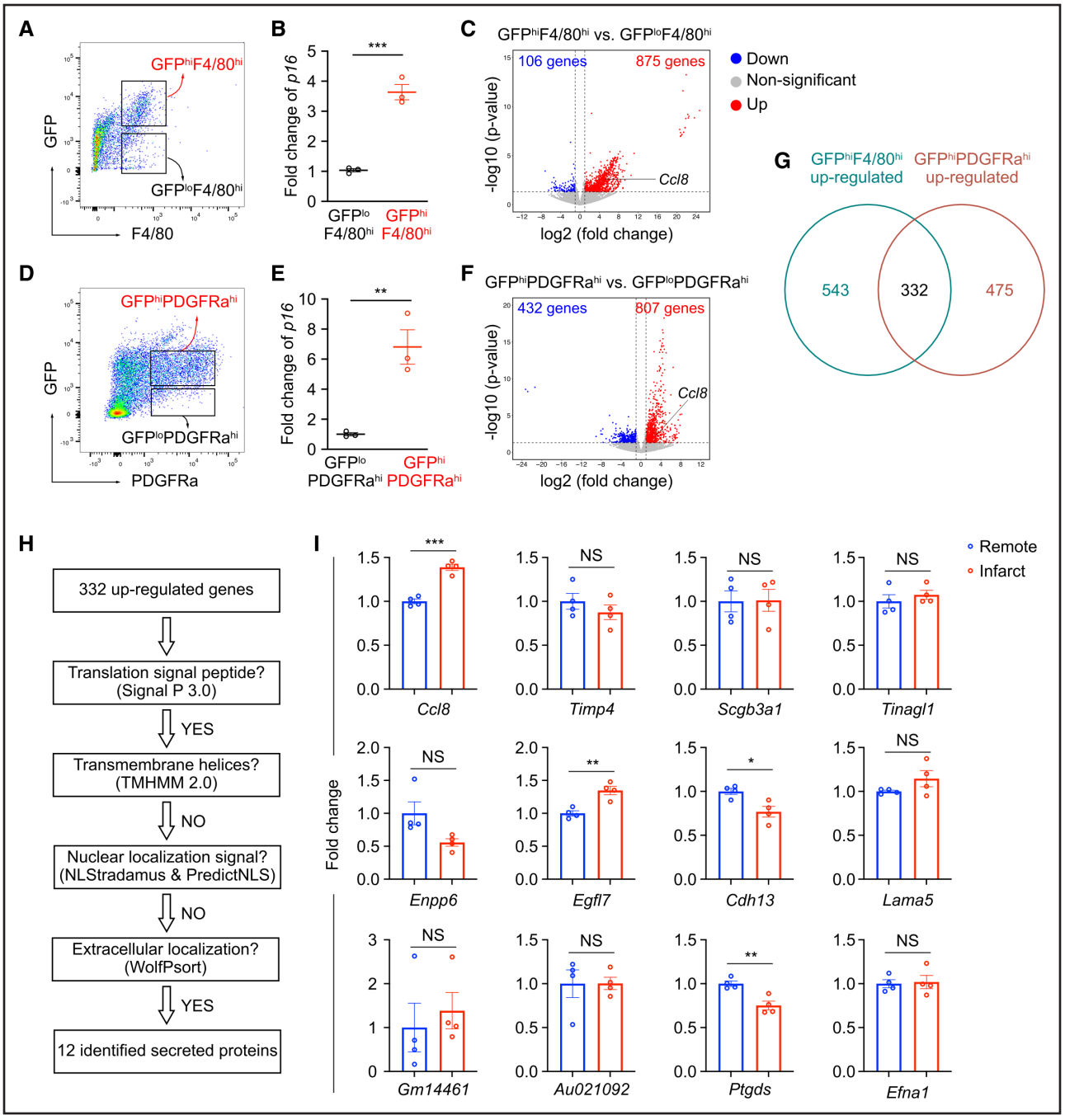

Figure 3. *Ccl8* expression is upregulated in P16+ macrophages and fibroblasts after MI.
A, GFP^{high} and GFP^{low} macrophages isolated from *p16-CreER;R26-mTmG* mice at 7 days after MI. **B**, Fold change in *p16* expression in GFP^{high} versus GFP^{low} macrophages. n=3 mice per group; ***P<0.001 (2-tailed Student t test). Both sexes were included. **C**, Differential expression analysis revealed 106 downregulated and 875 upregulated genes in GFP^{high} macrophages. *Ccl8* was upregulated (~33-fold). **D**, GFP^{high} and GFP^{low} fibroblasts isolated from *p16-CreER;R26-mTmG* mice 7 days after MI. **E**, Fold changes in *p16* expression in GFP^{high} versus GFP^{low} fibroblasts. n=3 mice per group; **P<0.01 (2-tailed Student t test). Both sexes were included. **F**, Differential expression analysis identified 432 downregulated and 807 upregulated genes in GFP^{high} fibroblasts. *Ccl8* was upregulated (~7-fold). **G**, A total of 332 genes coordinately upregulated in both GFP^{high} macrophages and fibroblasts. **H**, Bioinformatics pipeline for identifying secreted proteins among the 332 upregulated genes. **I**, Expression fold changes of candidate genes in infarct versus remote cardiac tissues. n=4 mice per group; NS, nonsignificant; *P<0.05; **P<0.01; ***P<0.001 (2-tailed Student t test). Both sexes were included. GFP^{hi} indicates GFP^{high}; GFP^{lo}, GFP^{low}; and MI, myocardial infarction.

outgoing signals to other cell types (Figure S8B). GFP^{high} and GFP^{low} fibroblasts similarly formed broad communication networks with outgoing signaling to other cell types (Figure S8C and S8D).

Focusing on CCL family ligand–receptor pairs, we detected CCL8-mediated outgoing signaling from GFP^{high} but not GFP^{low} macrophages (Figure 4F; Figure S9A). Recipient populations included endothelial cells,

ORIGINAL RESEARCH ARTICLE

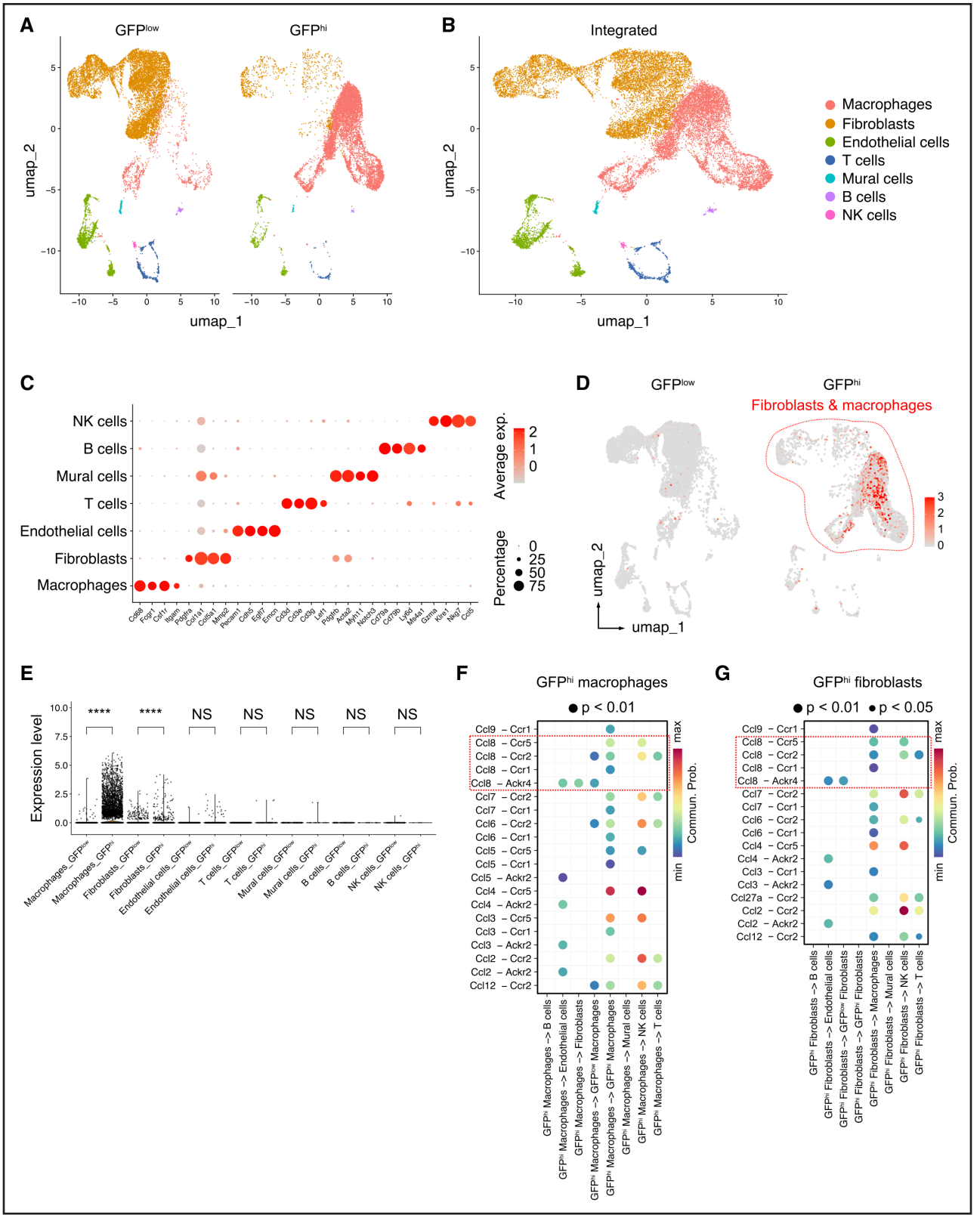

Figure 4. CellChat analysis identifies CCL8-mediated intercellular communication pathways in post-MI hearts.
A, UMAP visualization comparing cardiac cell populations between GFP^{hi} and GFP^{low} noncardiomyocyte cells from *p16-CreER;R26-mTmG* mice at 7 days after MI. Three mouse hearts were included per group. **B**, Integrated UMAP projection of major cardiac cell types from combined GFP^{hi} and GFP^{low} noncardiomyocyte cells. **C**, Dot plots displaying lineage marker gene expression for each cardiac cell population. Dot color and size indicate expression level and fraction of expressing cells, respectively. **D**, *Ccl8* expression in GFP^{hi} fibroblasts and macrophages. **E**, Violin plots depicting expression of *Ccl8* across cell populations in MI hearts. NS, nonsignificant; ****P<0.0001; statistical significance was (*Continued*)

Figure 4 Continued. determined by Wilcoxon test. **F** and **G**, Outgoing communication patterns of GFP^{hi} macrophages (**F**) and fibroblasts (**G**) through CCL signaling pathways. Dot color and size represent calculated interaction probability and *P* values, respectively. Red rectangles highlight CCL8-mediated interactions. CCL indicates cytokine (C-C motif) ligand; GFP^{hi}, GFP^{high}; MI, myocardial infarction; and UMAP, uniform manifold approximation and projection.

fibroblasts, NK cells, and T cells (Figure 4F). Analogously, CCL8-mediated signaling arose exclusively from GFP^{high} fibroblasts, with no detectable signaling from GFP^{low} fibroblasts, and targeted multiple cardiac cell types (Figure 4G; Figure S9B). Together, scRNA-seq and CellChat analyses establish P16^{+} macrophages and fibroblasts as the principal sources of CCL8-driven communication in post-MI hearts, coordinating crosstalk with diverse recipient cells.

We next examined the expression of CCL8 receptors in MI hearts using our integrated scRNA-seq dataset. Multiple CCL8 receptors—*Ackr4*, *Ccr1*, *Ccr2*, and *Ccr5*—were expressed across various noncardiomyocyte clusters (Figure S10A). Quantitative polymerase chain reaction further confirmed that all 4 receptors were significantly upregulated in infarcted regions versus sham-operated hearts (Figure S10B).

To define cell-type–specific changes in CCL8 receptor expression after MI, we analyzed a publicly available scRNA-seq dataset from sham and 7-day post-MI hearts (GSE266597). Uniform manifold approximation and projection identified 9 distinct clusters, each expressing established lineage markers (Figures S11A and S11B). We found that *Ackr4* was significantly elevated in fibroblasts after MI, *Ccr1* was markedly upregulated in macrophages, and *Ccr2* was strongly induced in macrophages, T cells, and NK cells. *Ccr5* expression was increased in macrophages and T cells but decreased in NK cells after MI (Figure S11C). These results further suggest that CCL8 produced by P16^{+} macrophages and fibroblasts may act on multiple cell types within the infarcted heart.

CCL8 Neutralization Enhances Cardiac Repair and Reduces Cytotoxic Lymphocyte Infiltration After MI

We next evaluated the role of CCL8 in remodeling after MI using a neutralizing antibody, administered at a dose of 20 µg per mouse weekly as adapted from previous studies (Figure 5A).[36] Compared with controls, CCL8 blockade significantly improved cardiac function (Figure 5B and 5C) and reduced fibrotic scar area (Figure 5D and 5E), indicating enhanced cardiac repair.

Because CCL8 is known to recruit CD8^{+} T cells and these cells accumulate in the infarcted myocardium (Figure S12A), we examined whether CCL8 blockade altered their infiltration. Both immunostaining and flow cytometry confirmed that CCL8 neutralization markedly reduced CD8^{+} T-cell accumulation in infarct regions (Figure 5F and 5G; Figure S12B and S12C), whereas immunostaining for CD4 showed no significant differences in CD4^{+} T-cell recruitment (Figure 5H and 5I).

We next examined NK cells, another cytotoxic subset recruited to infarcted myocardium after MI. NKp46 (natural cytotoxicity triggering receptor 1) immunostaining confirmed NK cell infiltration (Figure S12D), and these cells expressed the cytotoxic effectors perforin 1 (*Prf1*) and *Gzmb* (Figure S12E). Consistent with CellChat predictions linking CCL8 to NK cell recruitment (Figure 4F and 4G), CCL8 blockade reduced NK cell infiltration (Figure 5J and 5K; Figure S12F and S12G).

To evaluate dose dependency, we also tested higher antibody doses (30 µg and 40 µg per mouse weekly). Although these regimens similarly reduced CD8^{+} and NKp46^{+} cell recruitment into infarct regions (Figure S12H through S12O), the effects did not substantially exceed those achieved with the 20-µg dose. Therefore, the 20-µg weekly regimen was employed for analysis in all subsequent experiments.

Because both CD8^{+} T cells and NK cells mediate cytotoxicity, we evaluated cardiomyocyte apoptosis by c-CASP3 (cleaved caspase 3) immunostaining. CCL8 neutralization decreased c-CASP3^{+} cardiomyocyte density in infarct border zones (Figure 5L and 5M) and reduced GZMB expression in injured myocardium (Figure 5N and 5O). Together, these findings demonstrate that CCL8 blockade diminishes cytotoxic lymphocyte infiltration, suppresses GZMB expression, and alleviates cardiomyocyte apoptosis after MI.

To evaluate broader inflammatory states, we measured *Tnfα* expression, which was reduced in infarcted tissues of CCL8-neutralized mice (Figure 5P). By contrast, CD68 (macrophage marker) and MPO (myeloperoxidase; neutrophil marker) staining revealed comparable accumulation between groups (Figure 5Q and 5R), suggesting that diminished *Tnfα* likely reflects reduced cytotoxic lymphocyte activity rather than altered macrophage or neutrophil recruitment.

Analysis of coronary vasculature revealed no significant change in vascular density (Figure S13), indicating that CCL8 blockade does not substantially affect post-MI angiogenesis. Given the observed reduction in fibrotic scar area (Figure 5D and 5E) and the predicted interactions between CCL8 and fibroblasts (Figure 4F and 4G), we tested whether CCL8 directly modulates fibroblast activity. However, CCL8 treatment did not significantly alter the expression of major extracellular matrix genes (eg, *Col1a1*, *Col3a1*, *Postn*) (Figure S14A) and had no detectable effect on fibroblast proliferation or senescence in vitro (Figure S14B through S14E). Next, we isolated macrophages from post-MI hearts and examined

ORIGINAL RESEARCH ARTICLE

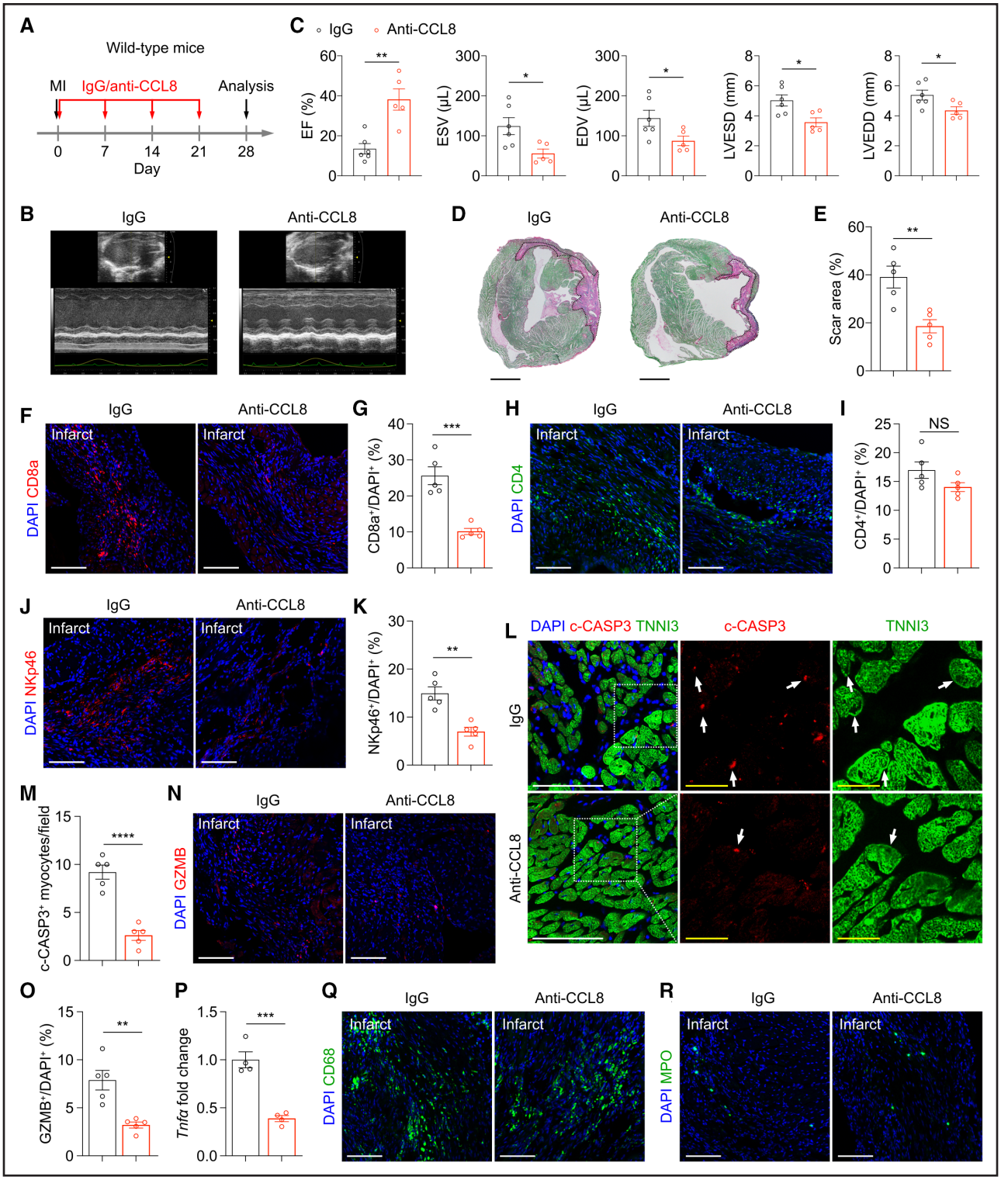

Figure 5. CCL8 neutralization improves cardiac repair and attenuates lymphocyte infiltration after MI.
A, Experimental timeline for anti-CCL8 antibody administration (20 μg per mouse, weekly) after MI. **B**, Representative echocardiographic images at 28 days after MI. **C**, Cardiac function at 28 days after MI. n=5 or 6 mice per group; *$P<0.05$; **$P<0.01$ (2-tailed Student *t* test). Both sexes were included. **D**, Sirius red staining of hearts at 28 days after MI. Fibrotic scars are delineated by dashed lines. Scale bars, 2 mm. **E**, Quantification of fibrotic scar area in MI hearts. n=5 mice per group; **$P<0.01$ (2-tailed Student *t* test). Both sexes were included. **F**, **H**, and **J**, Immunostaining for CD8a (**F**), CD4 (**H**), and NKp46 (**J**) in infarct regions at 28 days after MI. Scale bars, 100 μm. **G**, **I**, and **K**, Quantification of $CD8a^+$ (**G**), $CD4^+$ (**I**), and $NKp46^+$ (**K**) cell densities in infarct regions. n=5 mice per group; **$P<0.01$; ***$P<0.001$; NS, nonsignificant (2-tailed Student *t* test). Both sexes were included. **L**, Costaining of c-CASP3 and TNNI3 in border zones at 28 days after MI. Arrows indicate $c\text{-CASP3}^+$ cardiomyocytes. White scale bars, 100 μm; yellow scale bars, 25 μm. **M**, Quantification of $c\text{-CASP3}^+$ cardiomyocytes in border zones. n=5 mice per group; ****$P<0.0001$ (2-tailed Student *t* test). Both sexes were included. **N**, Immunostaining for GZMB in hearts at 28 days (*Continued*)

Figure 5 Continued. after MI. Scale bars, 100 µm. **O**, Quantification of GZMB+ signals in infarct regions. n=5 mice per group; ***P*<0.01 (2-tailed Student *t* test). Both sexes were included. **P**, *Tnfα* mRNA fold-changes in infarcted myocardium. n=4 mice per group; ****P*<0.001 (2-tailed Student *t* test). Both sexes were included. **Q** and **R**, Immunostaining for CD68 and MPO in hearts at 28 days after MI. Scale bars, 100 µm. c-CASP3 indicates cleaved caspase 3; CCL8, cytokine (C-C motif) ligand 8; GZMB, granzyme B; MI, myocardial infarction; and MPO, myeloperoxidase.

whether CCL8 influences their polarization. CCL8 treatment did not significantly alter the M1/M2 polarization ratio of these macrophages (Figure S15).

Genetic Ablation of *Ccl8* in P16+ Cells Attenuates Adverse Cardiac Remodeling After MI

To directly test the contribution of P16+-derived CCL8, we generated conditional *Ccl8* knockout mice (*Ccl8*$^{fl/fl}$) by flanking exon 2 with loxP sites and crossed them with *p16-CreER* mice to produce *p16-CreER;Ccl8*$^{fl/fl}$ mutants. Mutants and littermate *Ccl8*$^{fl/fl}$ controls received tamoxifen every 4 days after MI to induce *Ccl8* deletion in P16+ cells (Figure 6A). Compared with controls, mutants displayed improved cardiac function and reduced scar area (Figure 6B through 6D).

Both immunostaining and flow cytometry confirmed that deleting *Ccl8* in P16+ cells attenuated CD8+ T cell and NK cell infiltration in infarct regions (Figure 6E through 6H; Figure S16A through 16D). It also reduced c-CASP3+ cardiomyocyte density (Figure 6I and 6J) and GZMB levels (Figure 6K and 6L). *Tnfα* expression was significantly lower in mutants (Figure 6M), whereas macrophage and neutrophil accumulation remained unchanged (Figure 6N and 6O). Together, these findings indicate that genetic deletion of *Ccl8* in P16+ cells mitigates adverse remodeling by limiting cytotoxic lymphocyte infiltration and cardiomyocyte apoptosis.

We also observed prominent c-CASP3 signals in noncardiomyocyte areas of the infarct region in both control and mutant mice (Figure S16E). To determine whether *Ccl8* deletion affected apoptosis in specific noncardiomyocyte populations, we quantified apoptosis in fibroblasts, endothelial cells, and macrophages within the infarct zones. This analysis revealed no significant differences in apoptosis of any of these cell types between groups (Figures S16F through S16K). Therefore, *Ccl8* ablation in P16+ cells did not detectably alter the apoptosis rate of fibroblasts, endothelial cells, or macrophages.

CD8+ T-Cell Depletion Improves Cardiac Repair After MI

Because both CCL8 blockade and genetic *Ccl8* deletion reduced CD8+ T cell and NK cell infiltration, we next asked whether depleting either subset alone was sufficient to improve remodeling. Using antibody-mediated depletion (Figure S17A), anti-CD8a treatment significantly improved left ventricular ejection fraction (Figure S17B and S17C), decreased CD8+ T cell infiltration and GZMB levels (Figure S17D through S17G), and reduced apoptotic cardiomyocyte density in infarct border zones (Figure S17H and S17I). Macrophage and neutrophil accumulation remained unaffected (Figure S17J and S17K). In contrast, NK cell depletion with anti-NK1.1 antibody—tested across varying doses and administration routes—failed to improve cardiac function or reduce cardiomyocyte apoptosis compared with controls (Figure S18). These findings demonstrate that CD8+ T cells as key mediators of adverse post-MI remodeling.

Intersectional Genetic Ablation of P16+ Fibroblasts, but Not P16+ Macrophages, Promotes Repair

Because CCL8 originates from both P16+ macrophages and fibroblasts, we next asked whether selective ablation of either subset modulates post-MI repair. To achieve population-specific ablation, we used *Rosa26-loxP-stop-loxP-rox-stop-rox-tdTomato-2A-DTR* (hereafter *R26-lr-tdT-DTR*) mice,[37] in which DTR (diphtheria toxin receptor) expression is activated only by dual recombination with Cre and Dre (Figure 7A). Single recombinase activity does not induce DTR, and diphtheria toxin administration ablates only double-recombinase (DTR+) cells.[37]

We generated a *p16-DreER* knock-in line by inserting a 2A-DreER cassette into the terminal exon of the endogenous *Cdkn2a* locus (Figure S19A). Crossing with *H11-rox-stop-rox-tdTomato* (hereafter *H11-tdT*) reporters validated tamoxifen-inducible recombination: 2- and 12-month-old *p16-DreER;H11-tdT* mice exhibited age-dependent increases in tdTomato+ cells across multiple organs (Figure S19B and S19C). In post-MI hearts, tamoxifen induced tdTomato+ cells among fibroblasts, cVECs, macrophages, and cardiomyocytes (Figure S19D through S19G), paralleling the distribution in *p16-CreER;R26-tdT* mice (Figure 1C through 1F).

To selectively ablate fibroblasts or macrophages, we generated *p16-DreER;Pdgfra-CreER;R26-lr-tdT-DTR* mice and *p16-DreER;Cx3cr1-CreER;R26-lr-tdT-DTR* mice, respectively (Figure 7A and 7B).[38] Controls included *p16-DreER;R26-lr-tdT-DTR*, *Pdgfra-CreER;R26-lr-tdT-DTR*, and *Cx3cr1-CreER;R26-lr-tdT-DTR* mice. Echocardiography revealed comparable baseline function across groups (Figure S20A). After tamoxifen and diphtheria toxin administration, mice were analyzed at 28 days after MI (Figure 7C).

Immunostaining confirmed significant reductions in P16+ fibroblast density in *p16-DreER;Pdgfra-CreER;R26-lr-tdT-DTR* mice (Figure 7D and 7E) and

ORIGINAL RESEARCH ARTICLE

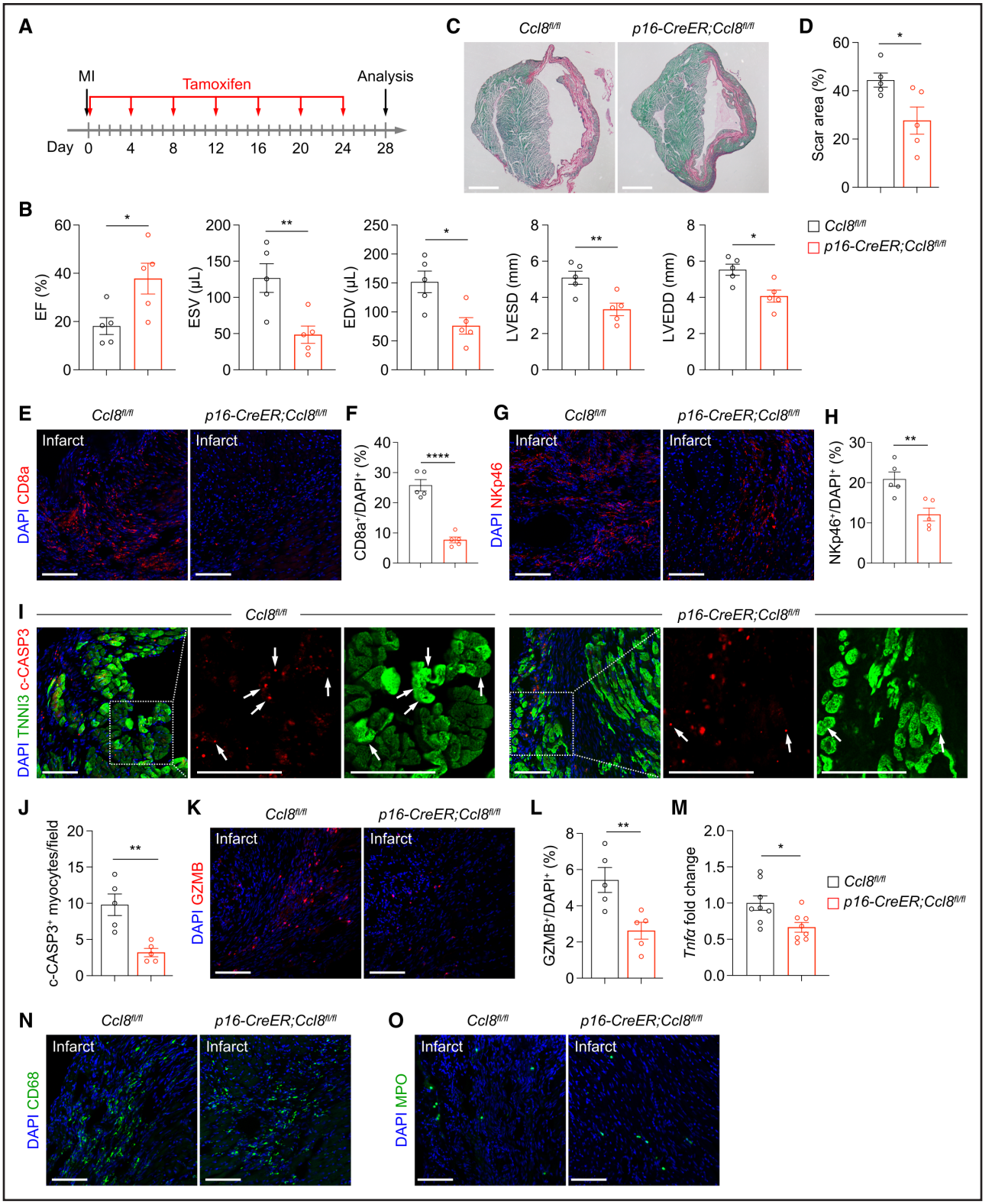

Figure 6. Genetic deletion of *Ccl8* in P16⁺ cells attenuates adverse post-MI cardiac remodeling.
A, Experimental timeline for tamoxifen-induced *Ccl8* deletion. **B**, Echocardiographic analysis at 28 days after MI. n=5 mice per group; **P*<0.05; ***P*<0.01 (2-tailed Student *t* test). Both sexes were included. **C**, Sirius red staining of hearts at 28 days after MI. Scale bars, 2 mm. **D**, Quantification of scar areas. n=5 mice per group; **P*<0.05 (2-tailed Student *t* test). Both sexes were included. **E**, Immunostaining for CD8a in hearts at 28 days after MI. Scale bars, 100 μm. **F**, CD8a⁺ cell density in infarct zones. n=5 mice per group; *****P*<0.0001 (2-tailed Student *t* test). Both sexes were included. **G**, Immunostaining for NKp46 in hearts at 28 days after MI. Scale bars, 100 μm. **H**, NKp46⁺ cell density in infarct regions. n=5 mice per group; ***P*<0.01 (2-tailed Student *t* test). Both sexes were included. **I**, Costaining of c-CASP3 and TNNI3 in border zones. Arrows indicate c-CASP3⁺ cardiomyocytes. White scale bars, 100 μm. **J**, c-CASP3⁺ cardiomyocyte density in border zones. (*Continued*)

Figure 6 Continued. n=5 mice per group; **P<0.01 (2-tailed Student t test). Both sexes were included. **K**, Immunostaining for GZMB in hearts at 28 days after MI. Scale bars, 100 µm. **L**, Quantification of GZMB+ signals in infarct regions. n=5 mice per group; **P<0.01 (2-tailed Student t test). Both sexes were included. **M**, *Tnfα* expression in injured myocardium. n=8 mice per group; *P<0.05 (2-tailed Student t test). Both sexes were included. **N** and **O**, Immunostaining for CD68 and MPO in hearts at 28 days after MI. Scale bars, 100 µm. c-CASP3 indicates cleaved caspase 3; GZMB, granzyme B; MI, myocardial infarction; and MPO, myeloperoxidase.

P16+ macrophage density in *p16-DreER;Cx3cr1-CreER;R26-lr-tdT-DTR* mice (Figure 7F and 7G). However, only *p16-DreER;Pdgfra-CreER;R26-lr-tdT-DTR* mice exhibited reduced scar area (Figure 7H and 7I) and improved heart function (Figure 7J; Figure S20B). Thus, selective ablation of P16+ fibroblasts—but not P16+ macrophages—promoted functional repair after MI.

DISCUSSION

In this study, we combined genetic mouse models with single-cell transcriptomics to systematically map P16+ cellular heterogeneity in the post-MI myocardium. We show that P16 is induced in fibroblasts, macrophages, cVECs, and cardiomyocytes after ischemic injury. Although P16 is widely used as a senescence marker, whether all P16+ cells in post-MI hearts are truly senescent remains unresolved; senescence may be confined to specific lineages, requiring further study. It is important to note that our findings shift the emphasis from senescence classification to functional consequences: P16+ macrophages and fibroblasts emerge as key drivers of adverse remodeling through convergent secretory programs. The pronounced heterogeneity among P16+ subsets suggests that P16 induction may serve lineage- and context-specific biological roles. The contributions of other P16+ populations to post-MI remodeling remain to be defined.

We identify P16+ macrophages and fibroblasts as the principal sources of CCL8 in infarcted hearts. Integrating intercellular communication analyses with functional studies, we delineate a CCL8-driven pathway in which these populations recruit cytotoxic lymphocytes, establishing a direct mechanistic link between P16+ stromal/immune cells and cardiomyocyte apoptosis. This aligns with observations in central nervous system injury, where microglia-derived CCL2/CCL8 chemokines mediate CD8+ T-cell infiltration and tissue damage in models of radiation-induced brain injury and ischemic stroke; conditional deletion of CCL2 or CCL8 prevents CD8+ T cell entry into the injured brain.[36] Whether CCL2 plays a similar role in post-MI CD8+ T cell recruitment remains to be determined. Our intercellular communication analyses also highlight other CCL ligands enriched in P16+ macrophages or fibroblasts, including CCL3, CCL5, and CCL12 (Figure 4F and 4G), which may modulate cytotoxic lymphocyte recruitment or activation. However, bulk RNA sequencing revealed no significant upregulation of *Ccl3*, *Ccl5*, or *Ccl12* in P16+ macrophages or fibroblasts relative to their P16− counterparts after MI. Defining the relative contributions of these chemokines to lymphocyte infiltration and subsequent remodeling represents an important direction for future work.

Our findings further demonstrate that P16+ cells recruit both CD8+ T cells and NK cells to infarcted myocardium. Antibody-mediated depletion experiments revealed that CD8+ T-cell removal mitigated adverse remodeling, whereas NK-cell depletion with anti-NK1.1 did not improve function or reduce cardiomyocyte apoptosis. This divergence is consistent with established evidence that CD8+ T cells directly kill cardiomyocytes through the perforin–granzyme pathway.[14] In the present study, however, anti-NK1.1 treatment reduced NK-cell infiltration by only approximately half, and incomplete depletion may limit the interpretation of their functional contribution. Thus, whether NK cells exert cytotoxicity comparable to that of CD8+ T cells during MI progression remains an open question that merits further investigation.

We speculate that the specific upregulation of CCL8 within P16+ macrophages and fibroblasts likely results from the convergence of cell-intrinsic senescent programming and injury-specific microenvironmental signals. First, P16+ populations are heterogeneous and likely contain a subset of senescent cells; thus, CCL8 could be a core component of the senescence-associated secretory phenotype (SASP) in the heart.[39] Ischemic stress-induced cellular senescence may thus directly activate *Ccl8* transcription alongside other classic SASP factors, positioning it as a programmed response that promotes immune cell recruitment. Second, the postinfarct milieu—characterized by hypoxia and the release of primary inflammatory mediators (eg, IFN-γ [interferon γ], TNFα [tumor necrosis factor α], and IL [interleukin] 1β])—also likely provides additional signals through master regulators such as NF-κB (nuclear factor κB) or STAT1 (signal transducer and activator of transcription 1), which are known to drive *Ccl8* expression.[40] Last, the cell type–specific amplification in macrophages and fibroblasts may stem from their central roles in the injury response, in which innate signaling pathways—such as Toll-like receptor signaling in macrophages and TGF-β (transforming growth factor β) signaling in fibroblasts—synergize with the above mechanisms to further amplify *Ccl8* expression.[41,42] Thus, CCL8 upregulation is probably not the result of a single trigger but rather a multifactorial response in which diverse signals synergistically shape the chemokine landscape of the injured heart. This hypothesis, although it requires formal validation,

ORIGINAL RESEARCH ARTICLE

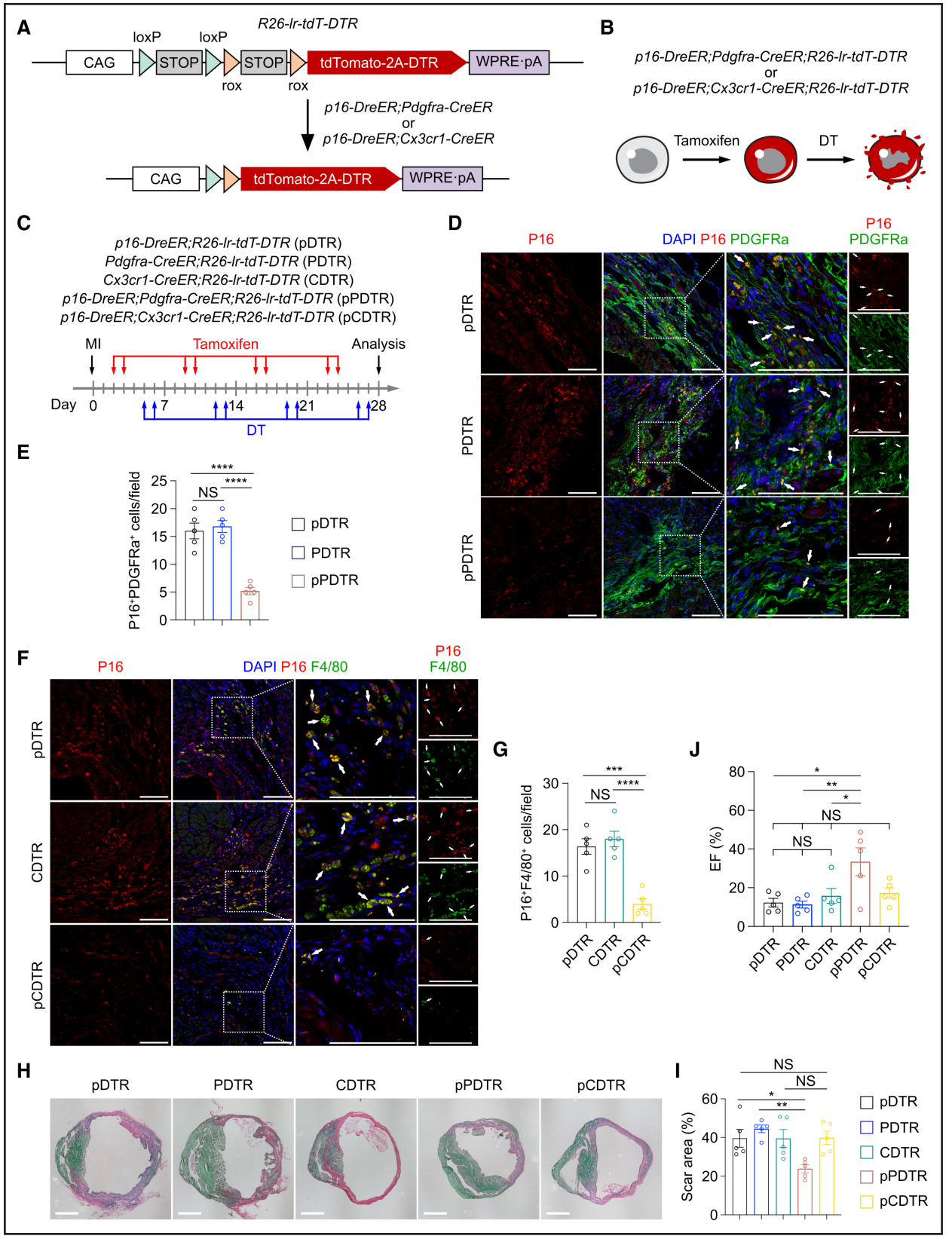

Figure 7. Ablation of P16⁺ fibroblasts, but not P16⁺ macrophages, promotes cardiac repair.
A, Schematic of the intersectional genetic strategy to ablate P16⁺ fibroblasts or macrophages. **B**, Sequential tamoxifen and DT treatment induces apoptosis of P16⁺ fibroblasts or macrophages. **C**, Experimental timeline for post-MI ablation. **D**, Immunostaining for P16 and PDGFRa in hearts at 28 days after MI. Arrows denote P16⁺ fibroblasts. Scale bars, 100 μm. **E**, Quantification of P16⁺ fibroblasts in infarct regions. n=5 mice per group; NS, nonsignificant; ****P<0.0001 (1-way ANOVA with Tukey multiple comparison test). Both sexes were included. (*Continued*)

Figure 7 Continued. **F**, Immunostaining for P16 and F4/80 in hearts at 28 days after MI. Arrows denote P16+ macrophages. Scale bars, 100 μm. **G**, Quantification of P16+ macrophages in infarct regions. n=5 mice per group; NS, nonsignificant; ***$P<0.001$; ****$P<0.0001$ (1-way ANOVA with Tukey multiple comparison test). Both sexes were included. **H**, Sirius red staining of hearts at 28 days after MI. Scale bars, 2 mm. **I**, Quantification of scar area at 28 days after MI. n=5 mice per group; NS, nonsignificant; *$P<0.05$; **$P<0.01$ (1-way ANOVA with Tukey multiple comparison test). Both sexes were included. **J**, Echocardiographic analysis of heart function at 28 days after MI. n=5 mice per group; NS, nonsignificant; *$P<0.05$; **$P<0.01$ (1-way ANOVA with Tukey multiple comparison test). Both sexes were included. DT indicates diphtheria toxin; and MI, myocardial infarction.

provides a mechanistic framework for our findings and suggests directions for further investigation.

Genetic deletion of *Ccl8* in P16+ cells improved cardiac repair, but this should not be equated with the effects of global P16+ cell clearance. Targeted gene deletion and wholesale cellular ablation represent distinct interventions with potentially divergent outcomes. Here we demonstrate that selective ablation of P16+ fibroblasts enhanced cardiac function and reduced fibrotic scar area after MI, consistent with previous reports that diphtheria toxin–mediated elimination of periostin-positive fibroblasts reduces fibrosis and improves cardiac performance.[43] Beyond MI, targeted fibroblast elimination using CAR (chimeric antigen receptor) T cells or CAR macrophages has been shown to promote repair in other cardiac pathologies.[44–47] It is important to note that excessive fibroblast loss may predispose to ventricular rupture or worsen outcomes.[48] In our model, however, we did not observe rupture or increased mortality, indicating that selective ablation of P16+ fibroblasts alone is insufficient to trigger rupture under the tested conditions.

Fibroblasts are the primary effector cells responsible for cardiac fibrosis after injury. Sustained fibrotic remodeling disrupts tissue architecture, reduces ventricular compliance, and impairs electromechanical function, ultimately contributing to heart failure.[49] Previous studies indicate that inhibiting fibroblast activation or depleting fibroblast numbers attenuates fibrosis and improves cardiac recovery.[43–47,50] In this context, P16+ fibroblasts represent a subpopulation that contributes to extracellular matrix production and expresses profibrotic mediators (Figure S6B through S6D); selective elimination of this subset may therefore help mitigate excessive scarring and support functional repair. Moreover, the P16+ fibroblast population likely contains a senescent subfraction, which could act as active signaling hubs through the SASP and dysregulate the injury microenvironment. For example, these cells may secrete TGF-β, PDGF, and other fibrogenic factors that activate neighboring fibroblasts (Figure S6C), further driving myofibroblast differentiation and extracellular matrix overproduction. Through inflammatory SASP components (eg, IL-6, TNFα), they could promote a proinflammatory milieu, inhibit endothelial cell migration and tube formation, and compromise reparative angiogenesis. SASP factors such as TNFα may also induce apoptosis in nearby cardiomyocytes, extending injury beyond the initial infarct zone. Our CellChat analysis further supports a role for P16+ fibroblasts

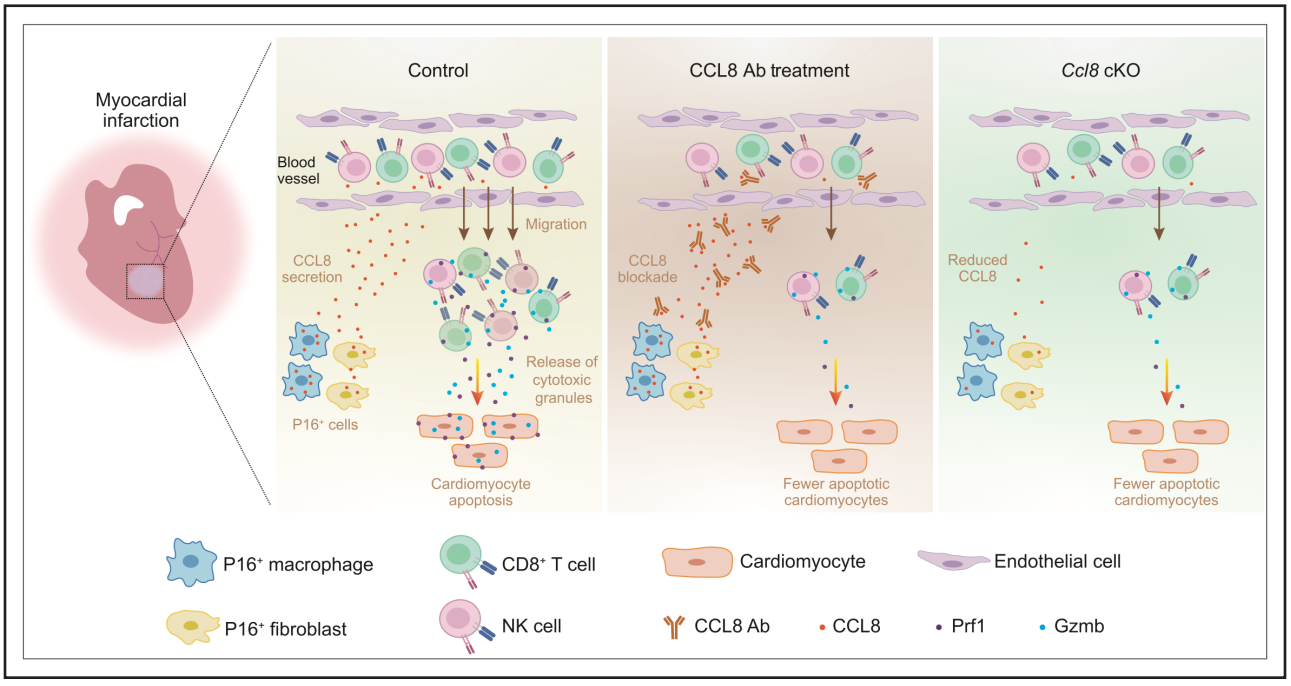

Figure 8. P16+ cells recruit cytotoxic lymphocytes through CCL8, driving cardiomyocyte apoptosis and adverse remodeling after MI.
CCL8 indicates cytokine (C-C motif) ligand 8; and MI, myocardial infarction.

in coordinating intercellular communication, showing strong interaction potentials with other fibroblasts and endothelial cells (Figure S8C and S8D)—consistent with their putative role in modulating fibrosis and vascular remodeling. Collectively, P16+ fibroblasts likely contribute to post-MI remodeling not only through direct matrix deposition but also through paracrine signaling that sustains fibrosis, impairs angiogenesis, and perpetuates inflammation. Their selective clearance through senolytic intervention or genetic approaches may thus disrupt a key node within this maladaptive network, although the precise functional identity of this subset warrants further investigation.

Partial ablation of P16+ macrophages did not alter cardiac function or fibrosis. This might reflect the heterogeneity of cardiac macrophage subsets, which exert stage-dependent and often opposing functions during inflammation, proliferation, and maturation phases of infarct healing.[51,52] As P16 is expressed in both proinflammatory and reparative macrophages, eliminating P16+ subsets could yield context-dependent effects. Future work should define the contributions of distinct P16+ macrophage subsets through combinatorial fate mapping, transcriptomic profiling, and temporally controlled ablation.

Collectively, our findings position P16+ cells as central orchestrators of adverse post-MI remodeling through CCL8-mediated recruitment of cytotoxic lymphocytes (Figure 8). These data provide a mechanistic and cell type–specific framework for precision immunomodulation after MI. By moving beyond indiscriminate senolysis, our study highlights CCL8 blockade and selective targeting of P16+ fibroblasts as promising strategies to mitigate cytotoxic immunopathology, offering translational potential for ischemic heart disease.

ARTICLE INFORMATION

Received August 27, 2025; accepted January 30, 2026.

Affiliations

School of Life Science and Technology (L.Y., J.Z., A.Z., M.Y., J.M., H.Z.), State Key Laboratory of Advanced Medical Materials and Devices & Shanghai Clinical Research and Trial Center (H.Z.), ShanghaiTech University, China. State Key Laboratory of Cardiovascular Diseases and Medical Innovation Center, Shanghai East Hospital, Frontier Science Center for Stem Cell Research, School of Life Science and Technology, Tongji University, China (Z.L., J.T.).

Acknowledgments

We thank the Molecular Imaging Core Facility and the Molecular and Cell Biology Core Facility at the School of Life Science and Technology, ShanghaiTech University, for technical support. We also thank the staff members of the Integrated Laser Microscopy System and Animal Facility at the National Facility for Protein Science in Shanghai for providing technical support and assistance in data collection and analysis.

Sources of Funding

This work was sponsored by the National Key Research and Development Program of China (No. 2023YFA1800700), National Natural Science Foundation of China (No.s 32571300, 92268103, and 32322037), Fundamental Research Funds for the Central Universities (No. 22120240435), and Peak Disciplines (Type IV) of Institutions of Higher Learning in Shanghai.

Disclosures

None.

Supplemental Material

Supplemental Methods
Tables S1 and S2
Figures S1–S20

REFERENCES

1. Virani SS, Alonso A, Aparicio HJ, Benjamin EJ, Bittencourt MS, Callaway CW, Carson AP, Chamberlain AM, Cheng S, Delling FN, et al; American Heart Association Council on Epidemiology and Prevention Statistics Committee and Stroke Statistics Subcommittee. Heart disease and stroke statistics-2021 update: a report from the American Heart Association. *Circulation*. 2021;143:e254–e743. doi: 10.1161/CIR.0000000000000950
2. Liu T, Hao Y, Zhang Z, Zhou H, Peng S, Zhang D, Li K, Chen Y, Chen M. Advanced cardiac patches for the treatment of myocardial infarction. *Circulation*. 2024;149:2002–2020. doi: 10.1161/CIRCULATIONAHA.123.067097
3. Prabhu SD, Frangogiannis NG. The biological basis for cardiac repair after myocardial infarction: from inflammation to fibrosis. *Circ Res*. 2016;119:91–112. doi: 10.1161/CIRCRESAHA.116.303577
4. Swirski FK, Nahrendorf M. Cardioimmunology: the immune system in cardiac homeostasis and disease. *Nat Rev Immunol*. 2018;18:733–744. doi: 10.1038/s41577-018-0065-8
5. Hofmann U, Frantz S. Role of lymphocytes in myocardial injury, healing, and remodeling after myocardial infarction. *Circ Res*. 2015;116:354–367. doi: 10.1161/CIRCRESAHA.116.304072
6. Hofmann U, Frantz S. Role of T-cells in myocardial infarction. *Eur Heart J*. 2016;37:873–879. doi: 10.1093/eurheartj/ehv639
7. Martin P, Sanchez-Madrid F. T cells in cardiac health and disease. *J Clin Invest*. 2025;135:e185218. doi: 10.1172/jci185218
8. Hofmann U, Beyersdorf N, Weirather J, Podolskaya A, Bauersachs J, Ertl G, Kerkau T, Frantz S. Activation of CD4+ T lymphocytes improves wound healing and survival after experimental myocardial infarction in mice. *Circulation*. 2012;125:1652–1663. doi: 10.1161/CIRCULATIONAHA.111.044164
9. Weirather J, Hofmann UD, Beyersdorf N, Ramos GC, Vogel B, Frey A, Ertl G, Kerkau T, Frantz S. Foxp3+ CD4+ T cells improve healing after myocardial infarction by modulating monocyte/macrophage differentiation. *Circ Res*. 2014;115:55–67. doi: 10.1161/CIRCRESAHA.115.303895
10. Varda-Bloom N, Leor J, Ohad DG, Hasin Y, Amar M, Fixler R, Battler A, Eldar M, Hasin D. Cytotoxic T lymphocytes are activated following myocardial infarction and can recognize and kill healthy myocytes in vitro. *J Mol Cell Cardiol*. 2000;32:2141–2149. doi: 10.1006/jmcc.2000.1261
11. Yan X, Anzai A, Katsumata Y, Matsuhashi T, Ito K, Endo J, Yamamoto T, Takeshima A, Shinmura K, Shen W, et al. Temporal dynamics of cardiac immune cell accumulation following acute myocardial infarction. *J Mol Cell Cardiol*. 2013;62:24–35. doi: 10.1016/j.yjmcc.2013.04.023
12. Tang TT, Zhu YC, Dong NG, Zhang S, Cai J, Zhang LX, Han Y, Xia N, Nie SF, Zhang M, et al. Pathologic T-cell response in ischaemic failing hearts elucidated by T-cell receptor sequencing and phenotypic characterization. *Eur Heart J*. 2019;40:3924–3933. doi: 10.1093/eurheartj/ehz516
13. Voskoboinik I, Whisstock JC, Trapani JA. Perforin and granzymes: function, dysfunction and human pathology. *Nat Rev Immunol*. 2015;15:388–400. doi: 10.1038/nri3839
14. Santos-Zas I, Lemarie J, Zlatanova I, Cachanado M, Seghezzi JC, Benamer H, Goube P, Vandestienne M, Cohen R, Ezzo M, et al. Cytotoxic CD8(+) T cells promote granzyme B-dependent adverse post-ischemic cardiac remodeling. *Nat Commun*. 2021;12:1483. doi: 10.1038/s41467-021-21737-9
15. Ong S, Rose NR, Cihakova D. Natural killer cells in inflammatory heart disease. *Clin Immunol*. 2017;175:26–33. doi: 10.1016/j.clim.2016.11.010
16. Strassheim D, Dempsey EC, Gerasimovskaya E, Stenmark K, Karoor V. Role of inflammatory cell subtypes in heart failure. *J Immunol Res*. 2019;2019:2164017. doi: 10.1155/2019/2164017
17. Kumric M, Kurir TT, Borovac JA, Bozic J. The role of natural killer (NK) cells in acute coronary syndrome: a comprehensive review. *Biomolecules*. 2020;10:1514. doi: 10.3390/biom10111514
18. Ortega-Rodriguez AC, Marin-Jauregui LS, Martinez-Shio E, Hernandez Castro B, Gonzalez-Amaro R, Escobedo-Uribe CD, Monsivais-Urenda AE. Altered NK cell receptor repertoire and function of natural killer cells in patients with acute myocardial infarction: a three-month follow-up study. *Immunobiology*. 2020;225:151909. doi: 10.1016/j.imbio.2020.151909

19. Guo L, Wu D, Shen J, Gao Y. ERG mediates the inhibition of NK cell cytotoxicity through the HLX/STAT4/perforin signaling pathway, thereby promoting the progression of myocardial infarction. *J Physiol Biochem*. 2024;80:219–233. doi: 10.1007/s13105-023-00999-5
20. Baker DJ, Wijshake T, Tchkonia T, LeBrasseur NK, Childs BG, van de Sluis B, Kirkland JL, van Deursen JM. Clearance of p16Ink4a-positive senescent cells delays ageing-associated disorders. *Nature*. 2011;479:232–236. doi: 10.1038/nature10600
21. Burd CE, Sorrentino JA, Clark KS, Darr DB, Krishnamurthy J, Deal AM, Bardeesy N, Castrillon DH, Beach DH, Sharpless NE. Monitoring tumorigenesis and senescence in vivo with a p16(INK4a)-luciferase model. *Cell*. 2013;152:340–351. doi: 10.1016/j.cell.2012.12.010
22. Demaria M, Ohtani N, Youssef SA, Rodier F, Toussaint W, Mitchell JR, Laberge RM, Vijg J, Van Steeg H, Dolle ME, et al. An essential role for senescent cells in optimal wound healing through secretion of PDGF-AA. *Dev Cell*. 2014;31:722–733. doi: 10.1016/j.devcel.2014.11.012
23. Baker DJ, Childs BG, Durik M, Wijers ME, Sieben CJ, Zhong J, Saltness RA, Jeganathan KB, Verzosa GC, Pezeshki A, et al. Naturally occurring p16(Ink4a)-positive cells shorten healthy lifespan. *Nature*. 2016;530:184–189. doi: 10.1038/nature16932
24. Omori S, Wang TW, Johmura Y, Kanai T, Nakano Y, Kido T, Susaki EA, Nakajima T, Shichino S, Ueha S, et al. Generation of a p16 reporter mouse and its use to characterize and target p16(high) cells in vivo. *Cell Metab*. 2020;32:814–828.e6. doi: 10.1016/j.cmet.2020.09.006
25. Grosse L, Wagner N, Emelyanov A, Molina C, Lacas-Gervais S, Wagner KD, Bulavin DV. Defined p16(high) senescent cell types are indispensable for mouse healthspan. *Cell Metab*. 2020;32:87–99.e6. doi: 10.1016/j.cmet.2020.05.002
26. Zhao H, Liu Z, Chen H, Han M, Zhang M, Liu K, Jin H, Liu X, Shi M, Pu W, et al. Identifying specific functional roles for senescence across cell types. *Cell*. 2024;187:7314–7334.e21. doi: 10.1016/j.cell.2024.09.021
27. Zhang L, Pitcher LE, Yousefzadeh MJ, Niedernhofer LJ, Robbins PD, Zhu Y. Cellular senescence: a key therapeutic target in aging and diseases. *J Clin Invest*. 2022;132:e158450. doi: 10.1172/JCI158450
28. Farr JN, Xu M, Weivoda MM, Monroe DG, Fraser DG, Onken JL, Negley BA, Sfeir JG, Ogrodnik MB, Hachfeld CM, et al. Targeting cellular senescence prevents age-related bone loss in mice. *Nat Med*. 2017;23:1072–1079. doi: 10.1038/nm.4385
29. Chang J, Wang Y, Shao L, Laberge RM, Demaria M, Campisi J, Janakiraman K, Sharpless NE, Ding S, Feng W, et al. Clearance of senescent cells by ABT263 rejuvenates aged hematopoietic stem cells in mice. *Nat Med*. 2016;22:78–83. doi: 10.1038/nm.4010
30. Mehdizadeh M, Aguilar M, Thorin E, Ferbeyre G, Nattel S. The role of cellular senescence in cardiac disease: basic biology and clinical relevance. *Nat Rev Cardiol*. 2022;19:250–264. doi: 10.1038/s41569-021-00624-2
31. Chen MS, Lee RT, Garbern JC. Senescence mechanisms and targets in the heart. *Cardiovasc Res*. 2022;118:1173–1187. doi: 10.1093/cvr/cvab161
32. Dookun E, Walaszczyk A, Redgrave R, Palmowski P, Tual-Chalot S, Suwana A, Chapman J, Jirkovsky E, Donastorg Sosa L, Gill E, et al. Clearance of senescent cells during cardiac ischemia-reperfusion injury improves recovery. *Aging Cell*. 2020;19:e13249. doi: 10.1111/acel.13249
33. Madisen L, Zwingman TA, Sunkin SM, Oh SW, Zariwala HA, Gu H, Ng LL, Palmiter RD, Hawrylycz MJ, Jones AR, et al. A robust and high-throughput Cre reporting and characterization system for the whole mouse brain. *Nat Neurosci*. 2010;13:133–140. doi: 10.1038/nn.2467
34. Muzumdar MD, Tasic B, Miyamichi K, Li L, Luo L. A global double-fluorescent Cre reporter mouse. *Genesis*. 2007;45:593–605. doi: 10.1002/dvg.20335
35. Jin S, Guerrero-Juarez CF, Zhang L, Chang I, Ramos R, Kuan CH, Myung P, Plikus MV, Nie Q. Inference and analysis of cell-cell communication using CellChat. *Nat Commun*. 2021;12:1088. doi: 10.1038/s41467-021-21246-9
36. Shi Z, Yu P, Lin WJ, Chen S, Hu X, Chen S, Cheng J, Liu Q, Yang Y, Li S, et al. Microglia drive transient insult-induced brain injury by chemotactic recruitment of CD8(+) T lymphocytes. *Neuron*. 2023;111:696–710.e9. doi: 10.1016/j.neuron.2022.12.009
37. Wang H, He L, Li Y, Pu W, Zhang S, Han X, Lui KO, Zhou B. Dual Cre and Dre recombinases mediate synchronized lineage tracing and cell subset ablation in vivo. *J Biol Chem*. 2022;298:101965. doi: 10.1016/j.jbc.2022.101965
38. Parkhurst CN, Yang G, Ninan I, Savas JN, Yates JR 3rd, Lafaille JJ, Hempstead BL, Littman DR, Gan WB. Microglia promote learning-dependent synapse formation through brain-derived neurotrophic factor. *Cell*. 2013;155:1596–1609. doi: 10.1016/j.cell.2013.11.030
39. Suryadevara V, Hudgins AD, Rajesh A, Pappalardo A, Karpova A, Dey AK, Hertzel A, Agudelo A, Rocha A, Soygur B, et al. SenNet recommendations for detecting senescent cells in different tissues. *Nat Rev Mol Cell Biol*. 2024;25:1001–1023. doi: 10.1038/s41580-024-00738-8
40. Chavez B, Kiaris H. Insights on the role of the chemokine CCL8 in pathology. *Cell Signal*. 2025;134:111951. doi: 10.1016/j.cellsig.2025.111951
41. Struyf S, Proost P, Vandercappellen J, Dempe S, Noyens B, Nelissen S, Gouwy M, Locati M, Opdenakker G, Dinsart C, et al. Synergistic up-regulation of MCP-2/CCL8 activity is counteracted by chemokine cleavage, limiting its inflammatory and anti-tumoral effects. *Eur J Immunol*. 2009;39:843–857. doi: 10.1002/eji.200838660
42. Tominaga K, Suzuki HI. TGF-beta signaling in cellular senescence and aging-related pathology. *Int J Mol Sci* . 2019;20:5002. doi: 10.3390/ijms20205002
43. Kaur H, Takefuji M, Ngai CY, Carvalho J, Bayer J, Wietelmann A, Poetsch A, Hoelper S, Conway SJ, Mollmann H, et al. Targeted ablation of periostin-expressing activated fibroblasts prevents adverse cardiac remodeling in mice. *Circ Res*. 2016;118:1906–1917. doi: 10.1161/CIRCRESAHA.116.308643
44. Aghajanian H, Kimura T, Rurik JG, Hancock AS, Leibowitz MS, Li L, Scholler J, Monslow J, Lo A, Han W, et al. Targeting cardiac fibrosis with engineered T cells. *Nature*. 2019;573:430–433. doi: 10.1038/s41586-019-1546-z
45. Rurik JG, Tombacz I, Yadegari A, Mendez Fernandez PO, Shewale SV, Li L, Kimura T, Soliman OY, Papp TE, Tam YK, et al. CAR T cells produced in vivo to treat cardiac injury. *Science*. 2022;375:91–96. doi: 10.1126/science.abm0594
46. Gao Z, Yan L, Meng J, Lu Z, Ge K, Jiang Z, Feng T, Wang H, Liu C, Tang J, et al. Targeting cardiac fibrosis with chimeric antigen receptor macrophages. *Cell Discov*. 2024;10:86. doi: 10.1038/s41421-024-00718-4
47. Wang J, Du H, Xie W, Bi J, Zhang H, Liu X, Wang Y, Zhang S, Lei A, He C, et al. CAR-macrophage therapy alleviates myocardial ischemia-reperfusion injury. *Circ Res*. 2024;135:1161–1174. doi: 10.1161/CIRCRESAHA.124.325212
48. Kanisicak O, Khalil H, Ivey MJ, Karch J, Maliken BD, Correll RN, Brody MJ, SC JL, Aronow BJ, Tallquist MD, et al. Genetic lineage tracing defines myofibroblast origin and function in the injured heart. *Nat Commun*. 2016;7:12260. doi: 10.1038/ncomms12260
49. Travers JG, Kamal FA, Robbins J, Yutzey KE, Blaxall BC. Cardiac fibrosis: the fibroblast awakens. *Circ Res*. 2016;118:1021–1040. doi: 10.1161/CIRCRESAHA.115.306565
50. Kou S, Lu Z, Deng D, Ye M, Sui Y, Qin L, Feng T, Jiang Z, Meng J, Lin CP, et al. Activation of imprinted gene PW1 promotes cardiac fibrosis after ischemic injury. *Circulation*. 2025;151:623–639. doi: 10.1161/CIRCULATIONAHA.124.070738
51. Peet C, Ivetic A, Bromage DI, Shah AM. Cardiac monocytes and macrophages after myocardial infarction. *Cardiovasc Res*. 2020;116:1101–1112. doi: 10.1093/cvr/cvz336
52. Yap J, Irei J, Lozano-Gerona J, Vanapruks S, Bishop T, Boisvert WA. Macrophages in cardiac remodelling after myocardial infarction. *Nat Rev Cardiol*. 2023;20:373–385. doi: 10.1038/s41569-022-00823-5